RSC Advances

ROYAL SOCIETY OF CHEMISTRY

www.rsc.org/advances

Cite this: DOI: 10.1039/c0xx00000x

www.rsc.org/xxxxxx

ARTICLE TYPE

A Versatile Strategy to Fabricate MOFs/Carbon Materials Integrations and Their Derivatives for Enhanced Electrocatalysis

Xiao Ma,[a,b] Xue Zhao,[a,b] Jian Sun,[a] Dehui Li,[a,b] and Xiurong Yang*[a]

Received (in XXX, XXX) Xth XXXXXXXXX 20XX, Accepted Xth XXXXXXXXX 20XX

DOI: 10.1039/b000000x

We developed a new versatile strategy to fabricate metal–organic frameworks (MOFs)/carbon materials (CMs) integrations (rather than direct mixtures) based on non-selective adhesive action and bidentate chelating action of polydopamine (PDA) for the first time. More significantly, the resultant MOFs/CMs integrations can be bridged based on remaining self-polymerization action of dopamine. The final morphology of the integration depends on the shape of chosen CMs. Based on this strategy, we successfully synthesized a new 3D network composed of bridged multi-walled carbon nanotubes (MWCNTs) with omnibearing wrapped side-by-side ZIF-8 crystals (one typical MOF) on them. After calcination, the metal-free integration can be utilized as an oxygen reduction reaction (ORR) electrocatalyst without any modification. The most remarkable features of our catalyst are the high porosity derived from the remained ZIF-8 crystal structure, the sufficient and uniform exposed nitrogen-containing active sites derived from PDA and ZIF-8, and the extensive conductive pathway derived from the bridged MWCNTs support. As a result, our catalyst which is devoid of any metals exhibits high ORR activity comparable to that of existing state-of-the-art Pt/C catalyst in alkaline solution (half-wave potential of -0.19 V, current density of 5.68 mA cm^{-2}) as well as superior durability and tolerance to methanol than Pt/C catalyst.

Introduction

Metal–organic frameworks (MOFs) are an appealing family of porous crystals consisting of metal ion 'joints' and connecting organic 'struts'.[1, 2] Because of the ultrahigh porosity, various available compositions and easily governable pore structure, the derivatives of MOFs (or MOFs in conjunction with other function materials) can find considerable applications in energy, molecular storage/separation, sensing and drug delivery fields.[3-9] For example, very recently, various porous doped carbon (PDC) materials derived from one-step pyrolysis of MOFs/carbon materials (CMs) hybrids have been introduced as electrocatalysts of electrode reactions in fuel cell fields,[10-14] such as oxygen reduction reaction (ORR), oxygen evolution reaction and hydrogen evolution reaction. Here, the reason of the addition of CMs into MOFs system is that this combination can not only make full advantage of MOFs' merits, and enhance the conductivity[15, 16] of the catalyst system but also stop MOFs from collapsing availably during the indispensable annealing process.[17] Due to the superior conductivity and thermal stability as well as long-range ordering, carbon nanotubes and graphene are always selected to achieve the above object.[18] However, most endeavors in these fields are mainly devoted to replace CMs or try different MOFs containing different transition metals (such as Fe, Co and Ni), which depend on the M-N-C (M means metal) groups to obtain higher catalytic activity, and the majority of the synthetic methods are directly mixing (except Zhang et al. developed a two-dimension sandwich-like MOFs/graphene oxide compounds using polyvinyl pyrrolidone as a linker).[14] Due to the lack of available functional groups on CMs, the directly mixing method cannot connect MOFs and CMs effectively, nor can make them an organic integration. Therefore, there is no complete conductive pathway in the catalyst system, and the deserved synergistic effect is adversely affected. Besides, there have been a few reports on controlling the distribution of MOFs on the CMs or design of their overall configuration before. The majority of the reported catalyst systems are a random combination of the two components, which result in deficient and non-uniform exposed active sites on the catalyst surface. Consequently, most of their electrochemical activity cannot compare with the benchmark Pt/C catalyst. Therefore, there is a strong incentive to search for a new versatile strategy to connect MOFs and CMs effectively, and simultaneously control the distribution of MOFs on the CMs as well as build overall rational framework.

Dopamine (DA) is a kind of nitrogen-containing neurotransmitter possessing catechol groups. It will self-polymerize in alkaline solution with O_2. The produced polydopamine (PDA) is a non-selective, homogeneous and robust adhesive material for all solid substrates of any size. Since it was found by Messersmith et al., considerable efforts have been aimed at synthesizing multifunctional materials depending on PDA coating.[19] However, its ability of internal structural modification based on bidentate chelating action of the catechol

groups has remained largely unexplored.[20]

Herein, based on non-selective and homogeneous adhesive action as well as bidentate chelating action of PDA, we developed a universal strategy to connect MOFs and CMs effectively, making them an organic integration. More importantly, the resultant MOFs/CMs integration can be bridged based on the self-polymerization action of DA on different CMs. The final morphology of the integration will vary according to the shape of selected CMs. As we know, the coordination ability of individual phenolic hydroxyl group to metal ion is weak, here, we utilized two phenolic hydroxyl groups to capture metal ions.[21] Our strategy can simultaneously solve the problems of connection of MOFs and CMs, the distribution of MOFs on CMs as well as the catalyst system's internal configuration. Diffierent with the graphene, multi-walled carbon nanotubes (MWCNTs) can obtained by large-scale commercial production at low price. Therefore, we chose them as solid substrates, saving the time-cost greatly.[22] Meanwhile, $Zn(MeIM)_2$ (ZIF-8, MeIM = 2-methylimidazole) which possesses relatively high thermal stability and rich porosity was selected as an assembly precursor.[17, 23] Fortunately, we successfully synthesized a ZIF-8/MWCNTs integration, and after self-polymerization reaction of DA, a 3D network composed of MWCNTs with omnibearing wrapped side-by-side MOFs crystals on them was obtained for the first time. After pyrolysis, the integration transformed into PDC materials, which can be utilized as high performance electrocatalysts for ORR without any modification. Compared with other in situ synthesis methods, this method can not only introduce carbon and nitrogen sources by pyrolysis in one step, avoiding the traditional chemical vapor deposition (CVD) method that is expensive and tedious,[24] but also obtain high porosity derived from the retained ZIF-8 crystal structure as well as sufficient and homogeneous exposed nitrogen-containing active sites derived from PDA and ZIF-8. In addition, the employment of PDA can make the catalyst system a conductive network in all directions rather a simple mixture, producing better synergistic effect between MOFs and MWCNTs, and these features can greatly increase the catalytic rate of ORR. As a result, our catalyst which is devoid of M-N-C groups exhibits high ORR activity comparable to that of existing state-of-the-art Pt/C catalyst in alkaline solution. Furthermore, it also shows superior durability and tolerance to methanol (MeOH) than Pt/C catalyst.

Experimental section

Materials

MWCNTs (purity > 97 %, diameter: 20–40 nm, length: 1-2 μm) were purchased from Shenzhen Nanotech. Port Co. Ltd (NTP). Pt (20 % on carbon black) was purchased from Alfa Aesar. DA hydrochloride was purchased from Sigma-Aldrich Co. (St. Louis, USA). $Zn(NO_3)_2{\cdot}6H_2O$ and 2-MeIM were purchased from J & K Technology Co., Ltd. KOH and MeOH were brought from Beijing Chemical Reagent Company. Double-distilled (DI) water was prepared by the Milli-Q Pore water system (18.25 MΩ).

Synthesis of catalysts

The commercial MWCNTs (0.125 g) were refluxed in HNO_3 (250 mL 2.6 M) at 120 °C for 24 h.[25] The rinsed and dried MWCNTs (0.17 g) were dispersed in Tris–HCl (pH = 8.5, 0.01 M) (170 mL) solution, and then the mixture was sonicated for 10 min followed by adding DA hydrochloride (0.34 g) with stirring at room temperature for 24 h.[26] The solution was filtered and rinsed with distilled water followed by drying in a vacuum oven overnight at 80 °C. The resultant samples are denoted as MWCNTs-PDA.

The as-prepared MWCNTs-PDA (0.2 g) were dispersed in MeOH (15 mL) followed by ultrasonic for 10 min. Then, $Zn(NO_3)_2{\cdot}6H_2O$ (0.2231 g) and 2-MeIM (0.4926 g) were added successively in the resultant solution with stirring at 50 °C for 10 h.[27] The solution was filtered and rinsed with MeOH followed by drying in a vacuum oven overnight at 50 °C. The resultant samples are denoted as ZPC-1/1 (ZPC is the abbreviation of ZIF-8-PDA-MWCNTs and x/y means mass ratio of MWCNTs-PDA and ZIF-8). ZPC-0.5/1 and ZPC-2/1 were prepared under the same conditions but half or double the mass of MWCNTs-PDA was used. ZIF-8 crystals were prepared under the same conditions in the absence of MWCNTs-PDA. The as-prepared ZPC-0.5/1, ZPC-1/1, ZPC-2/1 were put in ceramic boats and then transferred to a tube furnace, pyrolyzed at 200 °C for 2 h and then pyrolyzed at 600 °C, 700 °C (not given), 800 °C, 900 °C and 1000 °C for 5 h respectively under argon flow.[5, 6] The as-prepared ZIF-8 was also put in a ceramic boat and then transferred to a tube furnace, pyrolyzed at 200 °C for 2 h and then pyrolyzed at 900 °C for 5 h under argon flow. The resultant products were immersed in H_2SO_4 (1 M) with stirring for 12 h followed by filtration and drying. The resultant samples are denoted as ZPC-x/y-T (T means the pyrolysis temperature) and ZIF-8-900 respectively.

Materials Characterization

Transmission electron microscopy (TEM) was executed with JEM-2000 FX operating at 200 kV accelerating voltage. Scanning electron microscopy (SEM) images were performed on a Philips XL 30 and a JEOL JSM-6700 F microscope. X-ray diffraction (XRD) analysis was carried out on a D/Max 2500 V/PC X-ray diffractometer with Cu radiation. X-ray photoelectron spectroscopy (XPS) measurements were carried out with an ESCALAB MK II photoelectron spectrometer (VG Co., UK) with Al Ka X-ray radiation as the X-ray source for excitation. Nitrogen sorption isotherms were measured at 77 K with a Quadra chrome adsorption instrument. Before analysis, the samples were degassed at 100 °C for 24 h. The specific surface areas were calculated using the BET method based on adsorption data in the relative pressure (P/P_0) range of 0.06-0.14 and the total pore volumes were determined from the amount of nitrogen adsorbed at a relative pressure (P/P_0) of 0.99. The pore size distributions (PSD) were determined via a nonlocal density functional theory (NL-DFT) method using nitrogen adsorption data. Raman spectra were carried out on a Renishaw Raman system model 2000 spectrometer. Thermogravimetric analysis (TGA) was obtained by NETZSCH STA 449 F3 Simultaneous TGA-DSC Instrument under N_2 atmosphere by 5 °C min^{-1}.

Electrochemical measurements

ORR measurements were carried out with a standard three-electrode system. A glassy carbon disk (d = 5.61 mm) and

platinum ring (d_1 = 6.50 mm, d_2 = 7.90 mm) rotating electrode (RRDE, Pine Instruments Co.) was used as the working electrode. An Ag/AgCl (saturated KCl) electrode (CH Instruments) was applied as the reference electrode and Pt plate was used as the counter electrode respectively. The volume of the cell is 318 cm^3, the volume of KOH (0.1 M) electrolyte is 200 mL for all experiments. The catalyst solution was prepared using 2 mg catalysts dispersed in 0.98 mL of ethanol and 0.02 mL of 5 wt. % Nafion solution followed by sonication treatment for 5 min. For all samples, the working electrode was made by loading 20 μL catalyst link onto the surface of glassy carbon disk (S = 0.2472 cm^2) followed by drying at room temperature. KOH (0.1 M) solution which was purged using an N_2/O_2 flow 30 min was used as electrolyte. The RRDE measurements were carried out on a MSRX speed controller (Pine Instruments Co.) and a CHI 660B electrochemical workstation (CH Instruments) with 1600 rpm for all experiments. The scan rate of the cyclic voltammetry (CV) and linear sweep voltammetry (LSV) is 100 mV s^{-1} and 10 mV s^{-1} respectively. The electron transfer number n and the H_2O_2 yields were calculated by eqn (1) and eqn (2):[28, 29]

$$n = \frac{4 \times I_D}{I_D + I_R / N} \quad (1)$$

$$H_2O_2\% = \frac{200 \times I_R}{I_D \times N + I_R} \quad (2)$$

Where I_D is the disk current, I_R is the ring current, and N is the collection efficiency (0.37).

The i_k was calculated by using the formula below:[30]

$$i_k = \frac{i_d \times i}{i_d - i}$$

where i is the measured current and i_d are the diffusion-limiting current respectively.

Calculation of Electrochemical Active Surface Area (EASA)

The EASA of Pt/C was calculated by using the formula below:[31]

$$\mathrm{EASA} = \frac{Q_H}{m \times q_H}$$

where Q_H is the integrating the charge of the hydrogen desorption region of CV diagram after double-layer correction, q_H is the charge of monolayer adsorption of hydrogen on a Pt surface which is assuming as 210 μC cm^{-2}. The specific EASA (the EASA per unit weight of metal) of the Pt/C was found to be 43.5 m^2/g. The real area of Pt/C catalyst (when the loading amounts is 0.04 mg) is 17.4 cm^2.

The EASA of ZPC catalysts was estimated using double-layer capacitor with following equation:[32]

$$C = A \times \frac{\varepsilon_r \times \varepsilon_0}{d} = (\int I \times d\,V) / \upsilon \times m \times V$$

in which ε_r is the electrolyte dielectric constant, ε_0 is the vacuum dielectric constant, d is the effective thickness of double layer, A is the EASA, I is the current density, V is the potential, υ is the potential scan rate and m is the mass of the ZPC catalyst on the electrode.

The EASA of the bare GCE (rotating disk electrode, Pine Instruments Co.) was calculated according to the literature, and the calculated surface area of bare GCE is 0.2 cm^2, which is well consistent with data provided by the company (0.196 cm^2). The CVs diagrams with different amounts of ZPC catalysts on GCE and the relationship between the loaded catalyst amounts and the capacitor were plotted in Figure S1†.The capacitors of ZPC-1/1-900 catalyst modified electrodes show a linear relationship with the corresponding EASA. The EASA of the ZPC-1/1-900 modified electrode (0.2 mg cm^{-2}) was calculated to be 5.60 cm^2.

Results and discussion

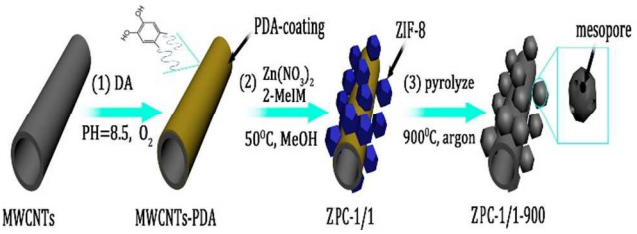

Scheme 1 The simple illustration of the preparation process of our PDC materials.

The formation process from MWCNTs with PDA coating to the organic integration and final PDC materials is illustrated schematically in Scheme 1. Firstly, in alkaline solution, the self-polymerization of DA would make them form a robust PDA coating on the MWCNTs. Secondly, the catechol groups of PDA would capture the zinc ions which were added subsequently. After the addition of 2-MeIM, ZIF-8 crystals would spontaneously form on the MWCNTs with strong coupling action in all directions. At this moment, the MWCNTs with ZIF-8 crystals growing on them began to close to each other based on the remaining polymerization force of DA. Finally, the 3D network composed of MWCNTs with omnibearing wrapped side-by-side MOFs crystals on them was successfully synthesized. Here, three mass ratios of MWCNTs-PDA and ZIF-8 which are 0.5:1, 1:1 and 2:1 were obtained. It is worth mentioning that, in order to control the size of ZIF-8 on the MWCNTs and reduce the steric hindrance, we elaborately chose the crystals obtained with Zn/MeIM in the known molar ratio of roughly 1: 8.[33]

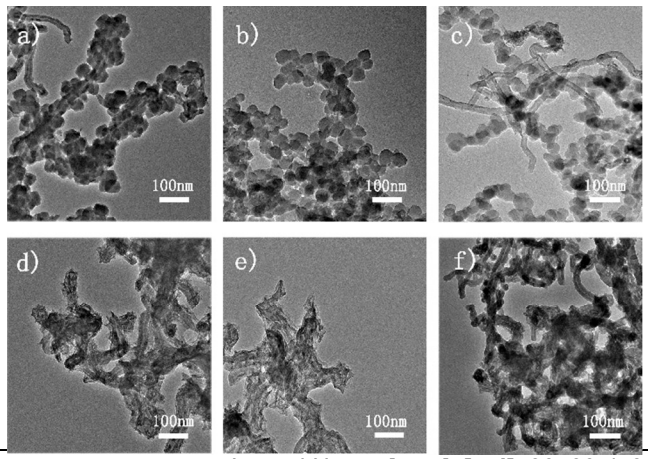

Fig. 1 TEM images of a) ZPC-0.5/1, b) ZPC-1/1, c) ZPC-2/1, d) ZPC-0.5/1-900, e) ZPC-1/1-900 and f) ZPC-2/1-900.

The morphology and structure of ZPC integration and PDC materials were characterized by TEM and XRD techniques. TEM images in Fig. 1 demonstrate that all of the ZIF-8 crystals successfully growed on the surface of MWCNTs uniformly, just like there are strong magnetic actions between the two components. Besides, when the increasing mass of the zinc ion and 2-MeIM were added into the MeOH solution with the same mass of MWCNTs-PDA, the resultant number of ZIF-8 crystals on MWCNTs is more and more, revealing that the growing process is gradual and controllable. Furthermore, because of the remaining inherent polymerization force of DA on the different MWCNTs, the MWCNTs with wrapped ZIF-8 crystals closed together to form 3D networks artfully. In this way, the framework support and the complete conductive pathway was constructed successfully. Here, probably owing to the crystals' interspersion by the catechol groups and the small space of each crystal, the shape of some ZIF-8 crystals are not a regular dodecahedron.[17] Furthermore, after carbonization, the original shape of the 3D networks was retained well, testifying the significance of supporting action of MWCNTs. The SEM images confirmed the above results from the perspective of three-dimensional (Fig. S2†). In addition, the corresponding element mappings of ZPC-1/1-900 are also given (Fig. S3 †), again indicating the homogeneous growth of ZIF-8 crystals on MWCNTs as well as the uniform distribution of nitrogen elements in PDC materials derived from PDA and ZIF-8 crystals. In order to prove the effect of MWCNTs, the pure ZIF-8 was also carbonized under the same conditions. The TEM images in Fig. S4 † show that, without the MWCNTs, the ZIF-8 crystals aggregated to form stacked carbon layers with irregular shape after carbonization. In this case, the nitrogen-containing active sites would be covered up, which is totally different from the pyrolysis of ZPC. Similarly, in order to demonstrate the effect of PDA, we also performed the experiment without it under the same conditions. The hybrid of ZIF-8 and MWCNTs were prepared by hydrothermal reaction for strengthening the interaction force between them (see support information). As given in Fig. S5†, the ZIF-8 crystals could hardly grow on the MWCNTs without PDA. After carbonization, the products were totally two phase, and the original structure have collapsed and the overall shape have not been retained well.

The XRD patterns verify that all the peak positions of the ZPC-1/1 are consistent with ZIF-8, indicating the crystals on the MWCNTs are indeed ZIF-8 (Fig. 2a). Moreover, the peak of ZPC-1/1-900 at 26.30 degree can also be attributed to the classic (002) crystal surface of sp^2-type carbon.[34] The graphitic qualities of ZIF-8-900 and ZPC-1/1-900 are evaluated by Raman spectroscopy techniques. The D band at 1360 cm^{-1} and G band at 1590 cm^{-1} in Raman spectra can give the information on disorder degree and crystalline degree of sp^2-type carbon respectively.[35] As shown in Fig. 2b, the I_D/I_G value of ZPC-1/1-900 is lower than that of ZIF-8-900, indicating that ZPC-1/1-900 has the higher crystalline degree of sp^2-type carbon. Here, we consider that the high crystalline degree of sp^2-type carbon can not only improve the electron transport but also induce the type conversion of the doped nitrogen which could enhance the activity of PDC materials for electrocatalysis.[34, 36]

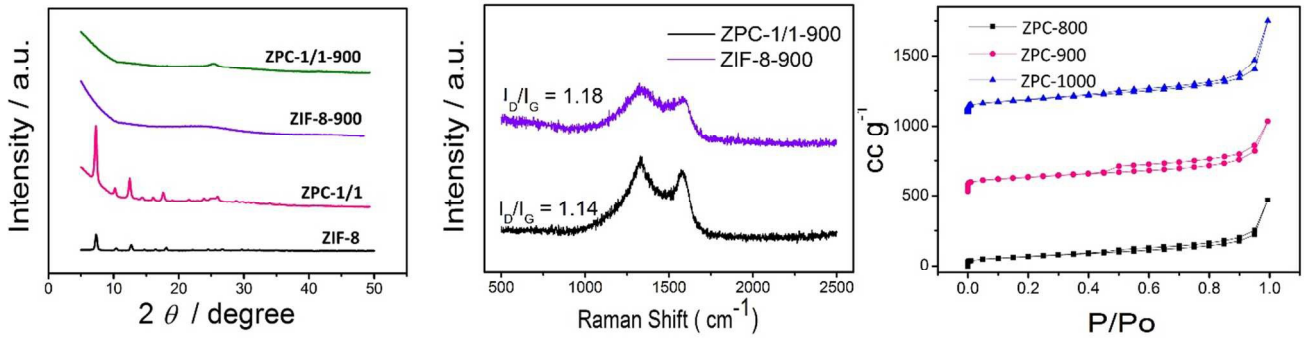

Fig. 2 a) The XRD patterns of ZIF-8, ZPC-1/1, ZIF-8-900, and ZPC-1/1-900; b) The Raman spectra of ZIF-8-900 and ZPC-1/1-900; c) Nitrogen adsorption/desorption isotherms of ZPC-1/1-800, ZPC-1/1-900 and ZPC-1/1-1000.

The N_2 adsorption-desorption isotherms of the PDC materials are shown in Fig. 2c. The curves of all the PDC materials show type-IV isotherms with hysteresis loop, indicating that ZPC-1/1-800, ZPC-1/1-900 and ZPC-1/1-1000 are of mesoporous structure.[37] The BET results exhibit that ZPC-1/1-900 has the highest specific surface area (352.72 $m^2\ g^{-1}$) among all PDC materials (the specific surface area of ZPC-1/1-800 is 293.48 $m^2\ g^{-1}$, and the specific surface area of ZPC-1/1-1000 is 308.46 $m^2\ g^{-1}$). Such numerical values could be attribute to the partial blocking in internal space of crystals caused by PDA. From the TGA in Fig. S6† we can observe that, PDA degraded gradually as the temperature increased, which could result in the release of internal space of crystals and could bring about the variation of specific surface area of MWCNTs-PDA. The PSD data of PDC materials are shown in Fig. S7 † , indicating that the PDC materials have uniform pore size of ~ 3.8 nm. The N_2 adsorption-desorption isotherms of MWCNTs-PDA, ZIF-8-900 and ZPC-1/1 are given in Fig. S8† for comparison.

The component of PDC materials was analyzed by the XPS techniques. The high-resolution N 1s spectra show that all the PDC materials exhibit three N chemical states, indicating that all the samples are nitrogen-doped carbon materials (Fig. 3). As shown in Table S1†, ZPC-1/1-900 has the highest content of N3 (quaternary-N), indicating that it owns the largest charge polarization degree in the carbon matrix, which would influence the electrochemical performance of the doped-carbon materials.[38] For example, in the from Table S1† and Fig. S9† we can obtain that ZPC-1/1-900 also has the highest content of crystalline degree of sp^2 carbon, which could advantageously affect the

electrochemical activity of PDC materials as mentioned above. Furthermore, the total nitrogen content of PDC materials decreased as the temperature increased. For comparison, the high-resolution N 1s spectra of ZIF-8-900,

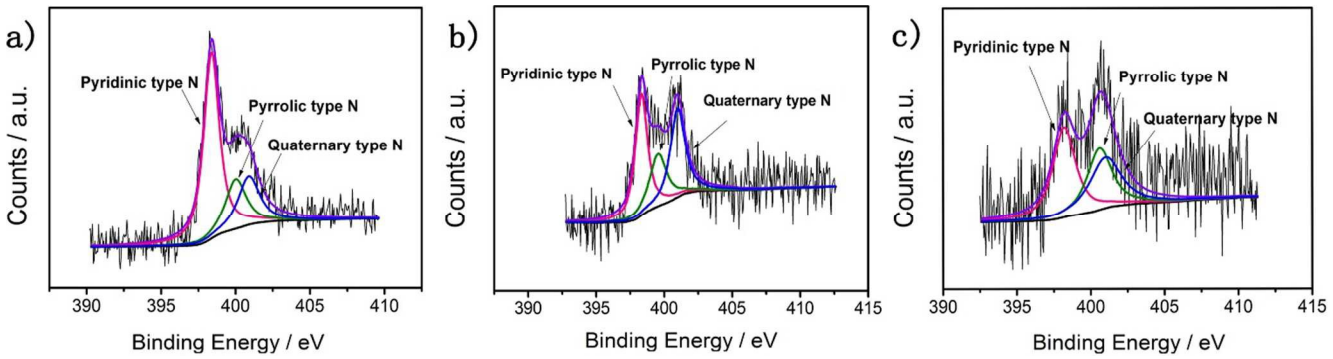

Fig. 3 The high-resolution N 1s spectra of a) ZPC-1/1-800, b) ZPC-1/1-900, and c) ZPC-1/1-1000.

MWCNTs-PDA, and ZPC-1/1 are shown in Fig. S10†.

Such PDC materials can be utilized as an electrocatalyst for ORR without any modification. The electrocatalytic activity of the PDC materials for ORR was tested by CV firstly (Fig. S11†). The CV curve of ZPC-1/1-900 displays an evident peak at ~ -0.2 V in O_2-saturated KOH solution (0.1 M), indicating that ZPC-1/1-900 possesses superior ORR catalytic activity. Furthermore, LSV was also performed on RRDE to evaluate the catalytic capability of catalysts.[41] As given in Fig. 4a, the curve shows that ZIF-8-900 has poor catalytic competence (onset potential of ~ -0.15 V, half-wave potential of ~ -0.29 V and current density of ~ 3.89 mA cm^{-2}). Unlike the ZIF-8-900, ZPC-1/1-900 has favorable performance (onset potential of ~ -0.08 V, half-wave potential of ~ -0.19 V and current density of ~ 5.68 mA cm^{-2}). The performance of ZPC-1/1-900 is similar to the benchmark Pt/C catalyst (onset potential of ~ -0.03 V, half-wave potential of ~ -0.17 V and current density of ~ 5.48 mA cm^{-2}) under the same conditions, demonstrating that after bridging with MWCNTs effectively, the electrocatalytic ability of the system is evidently much higher than that of pyrolysis products of pure ZIF-8 crystals. In order to give a better comparison to the commercial Pt/C catalyst, we calculated specific activity of our catalyst and the commercial Pt/C catalyst. As shown in Figure S12†, the specific activities of ZPC-1/1-900 is relatively higher than commercial Pt/C in 0.1M KOH solution at 0.164 V (vs. Ag/AgCl, saturated KCl, reference electrode). The transfer electron numbers of ZPC-1/1-900 catalyst at different potentials are ~ 3.7 - 3.8 (Fig. 4b), revealing that a dominant $4e^-$ reaction was mainly performed to reduce O_2 to OH^-. While, the transfer electron numbers of ZIF-8-900 are ~ 3.0 - 3.3 at different potentials, illustrating that the ORR process is a $2e^-$ and $4e^-$ combined reaction. Such results are also confirmed by the content of produced H_2O_2 by the catalysts (Fig. 4c). Furthermore, to the best of our knowledge, this effect cannot be achieve for the general PDC electrocatalysts in the absence of transition metals, except for vertically aligned N-containing CNTs (VA-NCNTs), which must be grown on a quartz substrate by CVD.[42] In order to compare with other contemporaries, we listed the performances of some outstanding electrocatalysts using electron transfer number and half-potential of LSV curve (Table S2), which were commonly utilized for characterizing the activity of electrocatalysts in ORR research fields.[43-51] Table S2 shows that our catalyst exhibits superior electrocatalytic property than these electrocatalysts, again proving that our method can produce higher active catalyst for ORR. We also explored the catalytic activity of the PDC catalysts obtained with the different mass ratios of MWCNTs-PDA and ZIF-8 crystals. From the Fig. 4d, we can obtain that ZPC-1/1-900 has the best performance, indicating that the appropriate number of crystals on the MWCNTs plays significant role for catalytic activity. We also investigated the catalytic activity of the PDC catalysts prepared at different temperatures. Figure 4 shows that ZPC-1/1-900 possesses the most positive half-wave potential and the highest current density. Such performance could results from the key factors including specific surface area, content of N3, crystalline degree of sp^2-type carbon and pore volume of PDC catalysts. The specific contributions of these four factors are given in Figure 5. As shown in Figure 5, ZPC-1/1-900 has the highest specific surface area, which could contribute to produce the biggest contact area to electrolyte. Meanwhile, it has the highest content of N3 that owns the largest charge polarization degree in the carbon matrix, which means it has the higher ability to absorb O_2.[38-40] In addition to the content of N3, ZPC-1/1-900 also has the highest content of sp^2-type carbon, which could not only contribute to improve of the conductivity, but also transform nitrogen atoms in five- or six-member ring.[7] PSD images in Figure S7† show that ZPC-1/1-900 almost have only the pore volume of ~3.8 nm, which is the biggest among other exist pores around 2.2 nm. The bigger pore volume could be more conducive to oxygen transmission.[52] Above four points are obviously conducive to enhance the ORR catalytic activity of ZPC-1/1-900. As for ZPC-1/1-800, although it has relatively high content of N3 and sp^2-type carbon, its specific surface area is relatively low and it has higher content of pores with ~2.2 nm, consequently, the catalytic effect is unsatisfactory. For ZPC-1/1-1000, N3 and sp^2-type carbon content of it reduced with the increasing temperature, and therefore, its catalytic activity was affected adversely. In order to further explore the influence of temperature on catalytic activity, we calculated the EASAs of the ZPC-1/1-800, ZPC-1/1-900 and ZPC-1/1-1000, which have a direct relationship with the catalytic properties and could also be affected by above four factors. The results reveal that ZPC-1/1-900 modified electrode has the largest EASA of 5.61 cm^2 with 0.2 mg cm^{-2} loading amount (the EASAs of ZPC-1/1-800, and ZPC-1/1-1000 modified electrodes are 3.47 cm^2 and 1.50 cm^2 respectively), which means that it have the most of active sites to participate in

the reaction, again demonstrating that 900 °C is the optimum temperature.

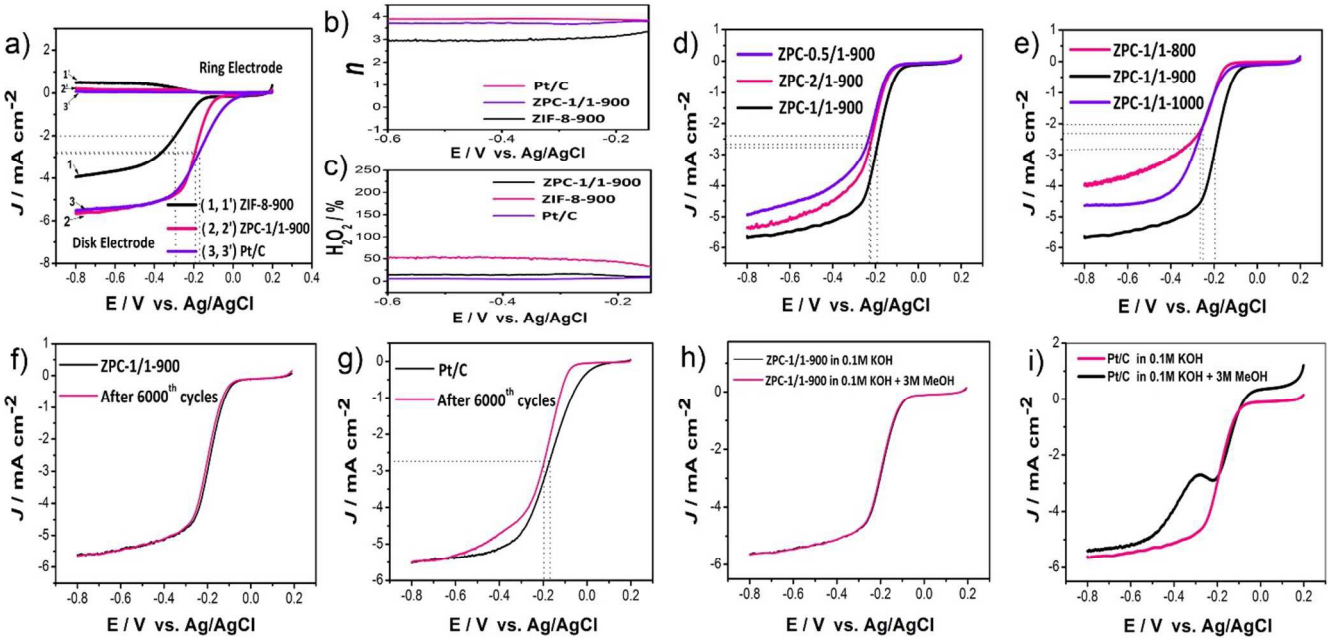

Fig. 4 a) The LSV curves of different catalysts in O_2-saturated 0.1 M KOH; b) Electron transfer number (n) of different catalysts at different potentials; c) Percentage of peroxide produced by different catalysts at different potentials; d) LSV curves of catalysts prepared by different mass ratios of MWCNTs-PDA and ZIF-8 in O_2-saturated 0.1 M KOH ; e) LSV curves of catalysts carbonized at different temperatures in O_2-saturated 0.1 M KOH ; f) LSV curve of ZPC-1/1-900 after 6000 cycles in O_2-saturated 0.1 M KOH; g) LSV curve of commercial Pt/C (20% on carbon black) after 6000 cycles in O_2-saturated 0.1 M KOH; h) LSV curve of ZPC-1/1-900 in O_2-saturated 0.1 M KOH and 3 M MeOH; i) LSV curve of benchmark Pt/C (20% on carbon black) in O_2-saturated 0.1 M KOH and 3 M MeOH. The sweep rate of all the LSV curves is 10 mV s^{-1}.

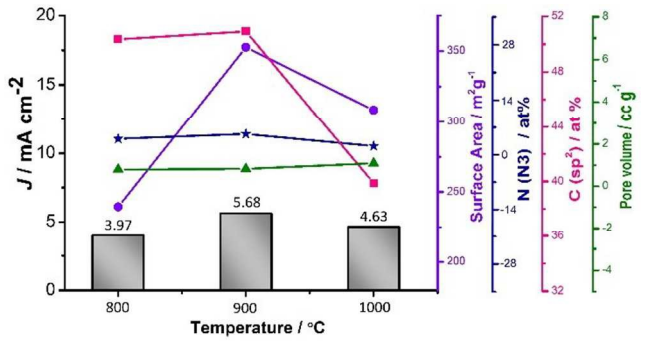

Fig. 5 Specific contributions of key factors which affect current density of ZPC-1/1-800, ZPC-1/1-900 and ZPC-1/1-1000.

In addition to the excellent ORR catalytic activity, ZPC-1/1-900 also shows superior stability. After 6000 sweep cycles from 0.2 V to -0.8 V in O_2-saturated KOH solution (0.1 M), the half-wave potential of ZPC-1/1-900 exhibited a negligible negative shift of ~ 1 mV (Fig. 4f), while the half-wave potential of benchmark Pt/C showed a remarkable negative shift of ~ 30 mV (Fig. 4g), revealing that ZPC-1/1-900 is more stable than the benchmark Pt/C catalyst under the alkaline conditions. Furthermore, ZPC-1/1-900 possesses superior tolerance to MeOH. After the addition of MeOH (3 M), no evident shift with the LSV curve of ZPC-1/1-900 was observed (Fig. 4h), which is very different from the Pt/C catalyst (Fig. 4i), demonstrating that such PDC catalyst is a promising alternative as a cathode catalyst for alkaline direct methanol fuel cell.

Conclusions

In summary, we developed a new versatile strategy to fabricate MOFs/CMs integrations based on non-selective adhesive action and chelating action of PDA. More significantly, the resultant MOFs/CMs integrations can be artfully bridged based on the remaining self-polymerization action of DA. Our strategy can not only solve the problem of MOFs' connection to the carbon support, the distribution of MOFs on CMs as well as the MOFs and CMs' overall configuration. Based on this method, we successfully fabricated a 3D network composed of bridged MWCNTs with omnibearing wrapped side-by-side ZIF-8 crystals on them. After calcination, it can be utilized as a metal-free electrocatalyst for ORR, which exhibits high activity comparable to that of existing state-of-the-art Pt/C catalyst in alkaline solution (half-wave potential of - 0.19 V, current density of 5.68 mA cm^{-2}). Furthermore, it also shows superior durability and tolerance to MeOH than Pt/C catalyst. Our work suggests that except M-N-C groups, the rational design of catalyst's internal configuration can also improve the reaction activity for electrocatalysts. Furthermore, due to the non-selectivity of PDA, this strategy could also be utilized to fabricate other MOFs/function materials integrations, which will have many applications in energy, molecular storage/separation, sensing and drug delivery fields.

Acknowledgements

This work was financially supported by the National Natural Science Foundation of China (No. 21175124, 21435005).

Notes and references

[a]*State Key Laboratory of Electroanalytical Chemistry, Changchun Institute of Applied Chemistry, Chinese Academy of Sciences, Changchun 130022, Jilin, China. E-mail: xryang@ciac.ac.cn*

[b]*University of the Chinese Academy of Sciences, Beijing 100049,China.*

†Electronic Supplementary Information (ESI) available: Experimental details, additional data and discussions. See DOI: 10.1039/b000000x/

1. O. M. Yaghi, M. O'Keeffe, N. W. Ockwig, H. K. Chae, M. Eddaoudi and J. Kim, *Nature*, 2003, **423**, 705-714.
2. D. J. Tranchemontagne, J. L. Mendoza-Cortes, M. O'Keeffe and O. M. Yaghi, *Chem. Soc. Rev.*, 2009, **38**, 1257-1283.
3. S.-Y. Liu, X.-L. Qi, R.-B. Lin, X.-N. Cheng, P.-Q. Liao, J.-P. Zhang and X.-M. Chen, *Adv. Funct. Mater.*, 2014, **24**, 5866-5872.
4. H. Furukawa, K. E. Cordova, M. O'Keeffe and O. M. Yaghi, *Science*, 2013, **341**, 974-986.
5. W. Zhang, Z.-Y. Wu, H.-L. Jiang and S.-H. Yu, *J. Am. Chem. Soc.*, 2014, **136**, 14385-14388.
6. L. J. Zhang, Z. X. Su, F. L. Jiang, L. L. Yang, J. J. Qian, Y. F. Zhou, W. M. Li and M. C. Hong, *Nanoscale*, 2014, **6**, 6590-6602.
7. S. Zhao, H. Yin, L. Du, L. He, K. Zhao, L. Chang, G. Yin, H. Zhao, S. Liu and Z. Tang, *ACS Nano*, 2014, **8**, 12660-12668.
8. J. L. Shui, C. Chen, L. Grabstanowicz, D. Zhao and D. J. Liu, *P. Natl. Acad. Sci. USA*, 2015, **112**, 10629-10634.
9. W. Yin, Y. Shen, F. Zou, X. L. Hu, B. Chi and Y. H. Huang, *ACS Appl. Mater. Interfaces*, 2015, **7**, 4947-4954.
10. M. Jahan, Z. L. Liu and K. P. Loh, *Adv. Funct. Mater.*, 2013, **23**, 5363-5372.
11. X. Z. Li, Y. Y. Fang, X. Q. Lin, M. Tian, X. C. An, Y. Fu, R. Li, J. Jin and J. T. Ma, *J. Mater. Chem. A*, 2015, **3**, 17392-17402.
12. J. Wei, Y. X. Hu, Z. X. Wu, Y. Liang, S. W. Leong, B. Kong, X. Y. Zhang, D. Y. Zhao, G. P. Simon and H. T. Wang, *J. Mater. Chem. A*, 2015, **3**, 16867-16873.
13. C. O. Ania, M. Seredych, E. Rodriguez-Castellon and T. J. Bandosz, *Appl. Catal. B-Environ.*, 2015, **163**, 424-435.
14. H.-X. Zhong, J. Wang, Y.-W. Zhang, W.-L. Xu, W. Xing, D. Xu, Y.-F. Zhang and X.-B. Zhang, *Angew. Chem., Int. Ed.*, 2014, **53**, 14235-14239.
15. S. Eslava, L. Zhang, S. Esconjauregui, J. Yang, K. Vanstreels, M. R. Baklanov and E. Saiz, *Chem. Mater.*, 2013, **25**, 27-33.
16. P. Ramaswamy, N. E. Wong and G. K. Shimizu, *Chem. Soc. Rev.*, 2014, **43**, 5913-5932.
17. K. S. Park, Z. Ni, A. P. Cote, J. Y. Choi, R. Huang, F. J. Uribe-Romo, H. K. Chae, M. O'Keeffe and O. M. Yaghi, *P. Natl. Acad. Sci. USA*, 2006, **103**, 10186-10191.
18. W. Yang, K. R. Ratinac, S. P. Ringer, P. Thordarson, J. Justin and F. Gooding, *Angew. Chem. Int. Ed.* 2010, **49**, 2114 – 2138.
19. H. Lee, S. M. Dellatore, W. M. Miller and P. B. Messersmith, *Science*, 2007, **318**, 426-430.
20. Y. Liu, K. Ai and L. Lu, *Chem. Rev.*, 2014, **114**, 5057-5115.
21. Q. Ye, F. Zhou and W. Liu, *Chem. Soc. Rev.*, 2011, **40**, 4244-4258.
22. V. Popov, *Mater. Sci. Eng., R*, 2004, **43**, 61-102.
23. J.-P. Zhang, Y.-B. Zhang, J.-B. Lin and X.-M. Chen, *Chem. Rev.*, 2012, **112**, 1001-1033.
24. H. T. Chung, J. H. Won and P. Zelenay, *Nat. Commun.*, 2013, **4**, 1922.
25. S. Guo, S. Dong and E. Wang, *Adv. Mater.*, 2010, **22**, 1269-1272.
26. X.-C. Liu, G.-C. Wang, R.-P. Liang, L. Shi and J.-D. Qiu, *J. Mater. Chem. A*, 2013, **1**, 3945-3953.
27. J.-B. Lin, R.-B. Lin, X.-N. Cheng, J.-P. Zhang and X.-M. Chen, *Chem. Commun.*, 2011, **47**, 9185-9187.
28. Y. Liang, Y. Li, H. Wang, J. Zhou, J. Wang, T. Regier and H. Dai, *Nat. Mater.*, 2011, **10**, 780-786.
29. M. Li, X. Bo, Y. Zhang, C. Han, A. Nsabimana and L. Guo, *J. Mater. Chem. A*, 2014, **2**, 11672-11682.
30. C. Kima, J. Oha, Y. Kimb, H. Kima and H. Leea, *Electrochem. Commun.* 2010, **12,** 1596–1599.
31. B. Lim, M. Jiang, P. H. C. Camargo, E. Cho, J. Tao, X. Lu, Y. Zhu and Y. Xia, *Science,* 2009, **324**, 1302-1305.
32. Y. Zhao, R. Nakamura, K. Kamiya and K. Hashimoto, *Nat. Commun.*, 2013, **4**, 2390.
33. J. Cravillon, R. Nayuk, S. Springer, A. Feldhoff, K. Huber and M. Wiebcke, *Chem. Mater.*, 2011, **23**, 2130-2141.
34. K. Ai, Y. Liu, C. Ruan, L. Lu and G. M. Lu, *Adv. Mater.*, 2013, **25**, 998-1003.
35. W. Yang, X. Liu, X. Yue, J. Jia and S. Guo, *J. Am. Chem. Soc.*, 2015, **137**, 1436-1439.
36. D.-W. Wang and D. Su, *Energ. Environ. Sci.*, 2014, **7**, 576-591.
37. P. I. Ravikovitch and A. V. Neimark, *Colloid. Sur. A-Physicochem. Eng. Asp.*, 2001, **187**, 11-21.
38. Y. She, Z. Lu, M. Ni, L. Li and M. K. Leung, *ACS Appl. Mater. Interfaces*, 2015, **7**, 7214-7221.
39. M. Shen, C. Ruan, Y. Chen, C. Jiang, K. Ai and L. Lu, *ACS Appl. Mater. Interfaces*, 2015, **7**, 1207-1218.
40. W. He, C. Jiang, J. Wang and L. Lu, *Angew. Chem., Int. Ed.*, 2014, **53**, 9503-9507.
41. D. Geng, Y. Chen, Y. Chen, Y. Li, R. Li, X. Sun, S. Ye and S. Knights, *Energ. Environ. Sci.*, 2011, **4**, 760-764.
42. K. P. Gong, F. Du, Z. H. Xia, M. Durstock and L. M. Dai, *Science*, 2009, **323**, 760–764.
43. S. Wohlgemuth, T. Fellinger, P. Jaker and M. Antonietti, *J. Mater. Chem. A,* 2013*, **1**, 4002-4009.*
44. A. Aijaz; N. Fujiwara and Q. Xu, *J. Am. Chem. Soc.*, 2014, **136**, 6790.
45. P. Zhang, F. Sun, Z. Xiang; Z. Shen, J. Yun, and D. Cao, *Energy Environ. Sci.*, 2014, *7*, 442-450.
46. L. J. Zhang, Z. X. Su, F. L. Jiang, L. L. Yang, J. J. Qian, Y. F. Zhou, W. M. Li and M. C. Hong, *Nanoscale*, 2014, **6**, 6590-6602.
47. W. Ai, Z. Luo, J. Jiang, J. Zhu, Z. Du, Z. Fan, L. Xie, H. Zhang, W. Huang, and T. Yu, *Adv. Mater.* 2014, **26**, 6186–6192.
48. J. Liang, Y. Jiao, M. Jaroniec, S.-Z. Qiao, *Angew. Chem. Int. Ed.* 2012, **51**, 11496-11500.
49. X. Zhao, H. Zhao, T. Zhang, X.Yan, Y. Yuan, H. Zhang, H. Zhao, D. Zhang, G. Zhu and X. Yao, *J. Mater. Chem. A,* 2014, **2**, 11666-11671.
50. S. Chen, J. Bi, Y. Zhao, L. Yang, C. Zhang, Y. Ma, Q. Wu, X. Wang and Z. Hu, *Adv. Mater.* 2012, **24**, 5593-5597.
51. Y. Zheng, Y. Jiao, J. Chen, J. Liu, J. Liang, A. Du, W. Zhang, Z. Zhu, S. C. Smith, M. Jaroniec, G. Q. Lu, and S. Qiao, *J. Am. Chem. Soc.* 2011, **133**, 20116–20119.
52. P. H. Matter, L. Zhang and U. S. Ozkan, *J. Catal.*, 2006, **239**, 83-96.

Graphical Abstract

Title

A Versatile Strategy to Fabricate MOFs/Carbon Materials Integrations and Their Derivatives for Enhanced Electrocatalysis

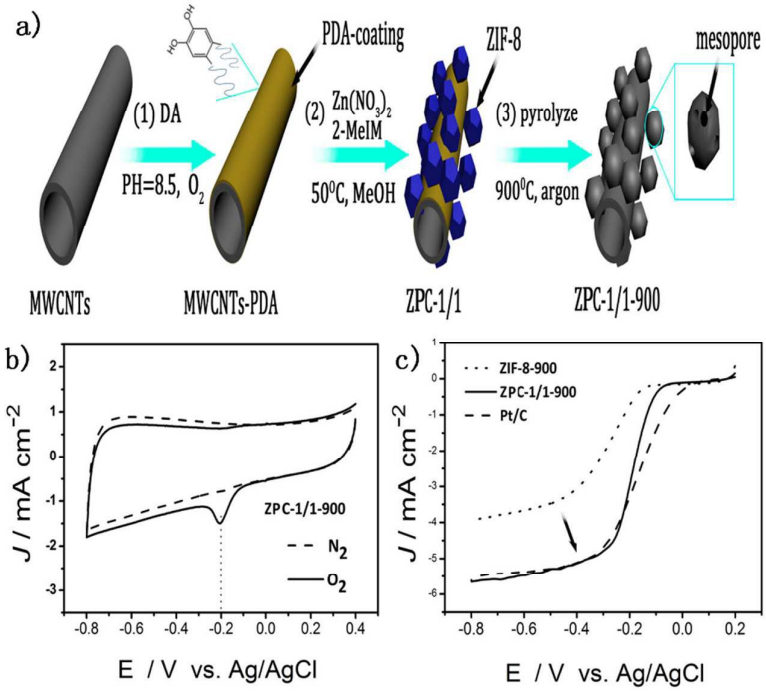

Fig.1 a) Illustration of the preparation of MOFs/carbon nanotubes integration and the derived catalyst; b) The CV curves of different catalysts in O_2 and N_2-saturated 0.1 M KOH. The sweep rate of CV curves is 100 mV s^{-1}; c) The LSV curves of different catalysts in O_2-saturated 0.1 M KOH at 1600 rpm. The sweep rate of LSV curves is 10 mV s^{-1}.